Single-Nanobelt Electronic Nose: Engineering and Tests of the Simplest Analytical Element

Victor V. Sysoev,[†] Evghenii Strelcov,[‡] Martin Sommer,[§] Michael Bruns,[§] Ilia Kiselev,[§] Wilhelm Habicht,[§] Swastik Kar,[⊥] Luca Gregoratti,[¶] Maya Kiskinova,[¶] and Andrei Kolmakov[‡,*]

[†]Saratov State Technical University, Saratov 410054, Russia, [‡]Southern Illinois University at Carbondale, Carbondale, Illinois 62901, [§]Karlsruhe Institute of Technology, 76344 Eggenstein-Leopoldshafen, Germany, [⊥]Rensselaer Polytechnic Institute, Troy, New York 12180, and [¶]Sincrotrone Trieste 34012 Trieste, Italy

ABSTRACT Electronic instruments mimicking the mammalian olfactory system are often referred to as "electronic noses" (E-noses). Thanks to recent nanotechnology breakthroughs the fabrication of mesoscopic and even nanoscopic E-noses is now feasible in the size domain where miniaturization of the microanalytical systems encounters principal limitations. Here we describe probably the simplest and yet fully functioning E-nose made of an individual single-crystal metal oxide quasi-1D nanobelt. The nanobelt was indexed with a number of electrodes in a way that each segment of the nanobelt between two electrodes defines an individual sensing elemental "receptor" of the array. The required diversity of the sensing elements is "encoded" in the nanobelt morphology *via* longitudinal width variations of the nanobelt realized during its growth and *via* functionalization of some of the segments with Pd catalyst. The proposed approach represents the combined bottom-up/top-down technologically viable route to develop robust and sensitive analytical systems scalable down to submicrometer dimensions.

KEYWORDS: SnO_2 nanobelt · nanosensor · nanowire electronic nose · gas recognition

The implementation of simple, cost-effective, power efficient, reliable, and sensitive nanodevices for real-time analysis of the ambient gas composition is currently a top design priority for environment pollution control, fossil fuel industry, automotive industry, medical research, and homeland security. To meet the strategic needs for development of novel sensing systems several approaches have been considered. The first one employs the recent progress in micromachining and microelectronics to scale down the dimensions of common analytical instruments such as ion mobility analyzers,[1] mass spectrometers,[2] optical spectrometers, gas chromatographs,[3] *etc.* Alternatively, there exists a biology-inspired approach[4,5] where the gas composition is recognized as an odor "fingerprint" or "pattern" rather than as a set of spectral features.[6] The typical system of this type exploits an array of partially specific artificial electrical (optical or mechanical) "receptors" coupled with pattern recognition techniques to process the multireceptor signals.[7] These electronic instruments, mimicking the mammalian (or insect) olfactory system are often referred to as "electronic noses" or E-noses.[8−10]

The idea to create an artificial "olfactory system" based on inexpensive electronic, optical, or mechanical devices has motivated extensive theoretical and experimental efforts over the past two decades.[6−10] However, it would be naïve to expect the artificial E-noses to achieve sensitivity and analytical power comparable even with one of the simplest insects, whose olfactory system has been perfected over millions of generations.[11] A number of already tested E-nose systems utilize a variety of receptor-transduction principles, such as FET-based,[12] SAW resonators,[13] micromechanical cantilevers,[14] optical fibers,[15] colorimetric arrays,[16] chemiresistors based on polymers,[17] and metal oxides,[6,8,10] as well as hybrid systems of diverse-typed sensors[18] and combinations of sensors with analytical instrumentation. The bottom-up paradigm of nanotechnology led to a reconsideration of approaches to design devices and their active elements.[19] The established high yield protocols for fabrication of quasi-one-dimensional (quasi-1D) nanostructures of traditional gas sensing materials, such as SnO_2, ZnO, In_2O_3,[20,21] have paved the way to use these metal oxide nano- and mesostructures such as nanowires, nanobelts (NB), nanoribbons, nanorods, whiskers, nanotubes, *etc.* as active elements in a number of nanoelectronic devices. (Here and below, unless specified, we are using the term "nanowire" (NW) in its generalized form implying the entire class of quasi-1D nanostructures). The most important properties that make these

***Address correspondence to akolmakov@physics.siu.edu.**

Received for review March 3, 2010 and accepted July 06, 2010.

Published online July 20, 2010. 10.1021/nn100435h

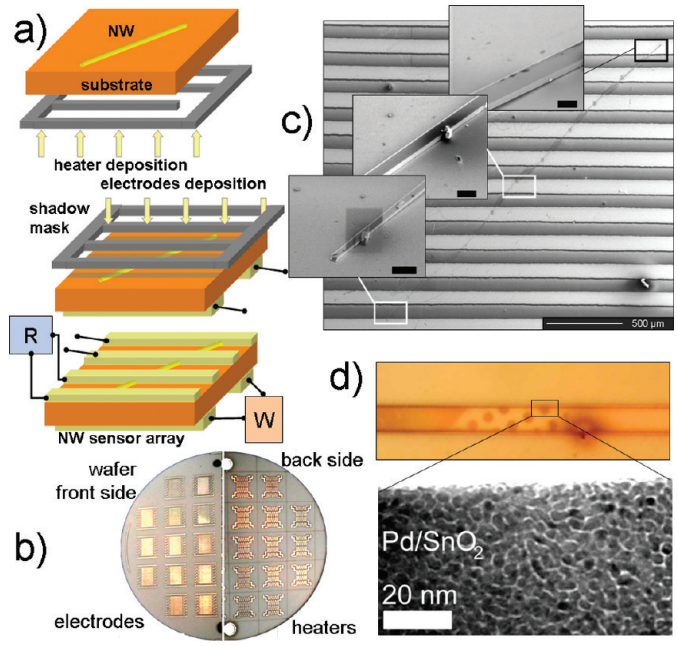

Figure 1. Fabrication and characterization of the single SnO_2 NB E-nose. (a,b) The deposition of Pt electrodes onto the individual NB and meander heaters onto the back of the Si/SiO_2 wafer. The ohm meter *R* and the power source *W* serve to conduct resistance measurements of the NB segments and heating of the substrate correspondingly. (c) Survey SEM image of the ultralong (*ca.* 1.5 mm) wedge-like SnO_2 nanobelt. The inset SEM images were taken at different locations along the NB and demonstrate the degree of the morphological changes (scale bar corresponds to 2 μm). (d) (Top) polarized optical microscopy images (×1000) of Pd patches deposited onto the three segments using the shadow mask; (bottom) TEM image of few ML Pd deposit indicates that the growth proceeds *via* Volmer−Weber (cluster) mode (for details see refs 30, 40).

semiconducting nanostructures nearly ideal building blocks for robust conductometric gas sensors (see reviews[22−24] and references therein) are (i) the generic chemical reactivity of their surfaces to a variety of gases; (ii) the large surface-to-volume ratio combined with an effective modulation of the nanostructure's conductance by the surface redox processes in the size domain where the radius of the nanostructure is comparable with the material's Debye length $L_D = (\varepsilon\varepsilon_0 kT/(e^2 n_0))^{1/2}$ (here ε and ε_0 are the dielectric constant of the material and permittivity of free space, correspondingly; e, k, and n_0 are electron charge, Boltzmann constant, and electron density, correspondingly); (iii) the single crystallinity of the nanostructure which offers limited number of facets exposed to the ambient (in case of a nanobelt it is effectively only one) and as a consequence the predictable modeling of the reactivity and transport properties; (iv) the microscopic length of the NBs which is sufficient for facile integration into resistor, diode, or FET (and their arrays[25]) device architecture and realization of sensing schemes with minimal power consumption.[26,27] Similar to their macroscopic counterparts (*e.g.*, thick- and thin-films)[28,29] the pristine metal oxide NB sensors are not particularly selective and possess cross sensitivity to a large number of gases. However, their chemical selectivity can be enhanced by surface functionalization with specific catalysts[30] and/or by tuning the temperature, guiding the design of sensor array for E-noses.[31,32]

On the basis of our prior[31,33] experience in design of nanowire based E-noses, here we describe a working and technologically viable proof-of-concept method to fabricate simple, robust, and stable miniature sensor arrays using an individual single crystal SnO_2 nanobelt as an active functional element.

RESULTS AND DISCUSSION

Device Fabrication. Tin oxide is well studied semiconducting oxide which traditionally serves as a testbench material to implement novel sensing principles and platforms in gas sensorics.[28,34,35] SnO_2 NBs were grown using a conventional vapor−solid method.[20,21] To avoid poisoning the surface adsorption sites with organic contaminants no wet protocols were used for device fabrication and NB manipulation (see Supporting Information Figures S1−S3). In particular, PVD *via* sputtering through the shadow masks in high vacuum (Figure 1a,b) or electron beam induced deposition (Figure 1c and Figures S4, S8) were used to fabricate Pt leads contacting the NB. These resist-free approaches resulted in inherently clean sensing elements beyond the electrode area that was proven by XPS and LEED[36] characterization of individual nanostructures and nearly ohmic contacts for the NB device (see Figures S2, S3 in the Supporting Information).

Parameters Variations along the Sensor Array. To provide a sufficient recognition power, the single NB analytical device requires diversity in the sensing performance of the individual sensing segments. To meet this require-

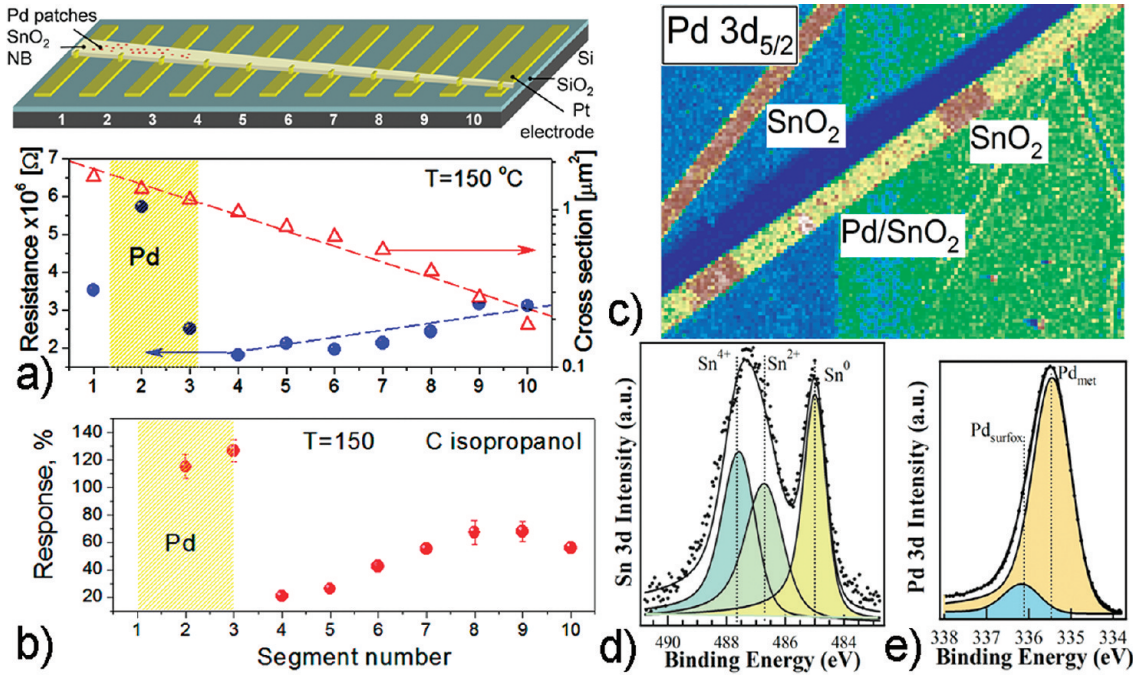

Figure 2. The schematic presentation of the single NB E-nose and variation of the NB parameters along its length. (a) The evolution of the resistance and geometrical cross section of the wedge-like NB (measured in vacuum at 150 °C) along its length. The resistance of first three Pd sensitized segments has an elevated value due to Pd induced electron depletion. For the undoped segments (4−10) the resistance increases steadily due to decrease of the cross section of the NB. (b) The sensor response of the individual segments of the NB at 150 °C to isopropyl alcohol, 50 ppm, mixed with a synthetic air. (c) SPEM image (45 × 64 μm², 500 nm step) of the Pd functionalized SnO_2 NB taken at Pd $3d_{5/2}$ photoelectrons. The color scheme defines the relative distribution of Pd at the surface of SnO_2 NB. The green background is the Pt electrode, and the blue one belongs to SiO_2/Si support. (d) The high resolution Pd 3d spectrum indicating the presence of surface PdO in dominating metallic Pd deposit. (e) The Sn 3d spectrum exhibits the presence of metallic Sn^0 as well as convoluted Sn^{2+} and Sn^{4+} peaks in the area of Pd patch.

ment few parameters of the NB were varied along its length: (i) the cross-section of the NB and (ii) the surface functionalization of the selected segments with Pd catalyst. The variation of the NB effective diameter *D* was achieved by slowly decreasing the SnO precursor flux into the condensation zone during the NB growth,[37] which resulted in growth of wedge-like NBs. When required, the surface of a few segments was doped with Pd patches by Pd evaporation through a shadow mask prior to the electrode deposition[30] (Figure 1d and Supporting Information, Figure S6). To avoid possible electrical conductance through the percolating Pd nanoparticles, the metal patches have separating gaps of the pristine SnO_2 between them (see bright dots and strips in Figure 1d and Supporting Information, Figure S7, correspondingly).

The dissociation and ionosorption of atmospheric oxygen at the surface active sites of slightly reduced SnO_2 NB leads to surface charging accompanied by the adsorbate-induced upward band bending eV_S. The latter induces a space charge electron depleted region (SCR) of the width $W = L_D(eV_s/(kT))^{1/2}$. SCR reduces the effective cross section of the NB conducting channel. When combustible analytes interact with ionosorbed oxygen on the surface, the oxygen coverage decreases modulating effectively the width of SCR and therefore the NB conductance. The response of the individual NB sensing segment (defined here as the ratio R_{air}/R of resistances of the NB in air R_{air} *versus* the one in air−analyte mixture *R*) depends on the *W/D* ratio. Consequently the variation of the effective diameter *D* of the NB along its length provides the required diversity in the sensitivity for each individual sensing segment. Since the modulation of *W/D* ratio is analyte specific, this gives sufficient gas specificity for every NB sensing segment which is necessary to provide a recognition ability of the entire array.

The surface doping of selected NB segments with Pd nanoparticles (Figure 1d) improves the performance of the NB analytical system *via* triggering the variation of two additional parameters along the NB length. Namely (i) the deposition of high-work-function Pd patches onto SnO_2 results in formation of local nano-Schottky barriers that increase further the aforementioned *W/D* ratio.[29,30,34,35] These results in the enhanced resistivity of the NB segments sensitized with Pd (see the first three segments at the indexed NB drawn in Figure 2a,b). In addition, (ii) due to a catalytic action of Pd nanoparticles the reactivity of Pd-doped segments to combustible gases like CO and H_2, *etc.* is enhanced.[28−30,35,38−40] As a result, while the sensor response at the pristine segments is controlled by the effective diameter of the nanostructure conducting channel, it appears significantly improved at the segments

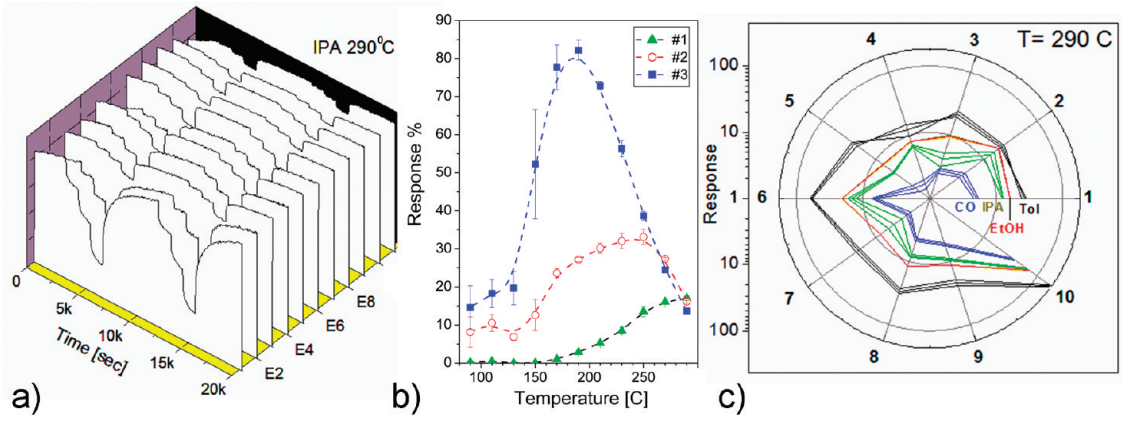

Figure 3. The performance of the single SnO_2 nanobelt E-nose. (a) The normalized resistances of the 10-segments (E1−E10) single NB E-nose operating at $T = 290$ °C to sequential exposure of 1, 5, and 30 ppm of isopropyl alcohol in the humidified (RH = 50%) air. (b) The typical dependencies of gas response of three (no. 1, 2, 3) various segments in the single NB E-nose *vs* operating temperature; test gas is 10 ppm of isopropyl alcohol in the humidified (RH = 50%) air. (c) The polar plot of response of the NB E-nose to four reducing gases (ethanol (Et), isopropyl alcohol (IPA), toluene (Tol), CO), 30 ppm concentration, mixed with humidified (RH = 50%) air.

sensitized with Pd (Figure 2a,b). The TEM image in Figure 1d shows that the growth of a few nm thick Pd deposits on the NB surface follows Volmer−Weber growth mode. The strong chemical interaction of Pd with SnO_2 is evident from the comparison of the deconvoluted Pd $3d_{5/2}$ and of Sn $3d_{5/2}$ spectra taken in spots outside and inside the Pd sensitized patch deposited onto the individual SnO_2 NB (Figure 2c−e and Supporting Information, Figure S7). The Pd $3d_{5/2}$ spectrum (Figure 2e) is rather broad which is typical for the cluster growth mode of Pd on SnO_2.[37] It is dominated by the metallic component at 335.5 eV and a small component shifted to higher binding energy by about 0.8 eV that can be attributed to the surface oxide.[38] The possible formation of surface Pd oxide is concomitant with the observed presence of the metallic component, Sn^0, in the Sn 3d spectra measured inside the Pd patch (Figure 2d), along with the SnO_2 and SnO components due to coexistence of both oxide phases, as already reported in ref 38. The reducing effect of Pd has already been noted in previous studies and has been explained in terms of weakening the Sn−O bonds resulting from Pd d- Sn s, p-orbital interactions (see review[35] and references therein).

The Performance of the Single Nanobelt E-Nose. The performance of more than a dozen single NB E-nose multisensors with and without Pd sensitization was tested. While functionalization with Pd catalyst is an apparent advantage, it requires extra steps in E-nose fabrication. It has been noticed that the fabrication protocol can be significantly simplified via direct R.F. sputtering of Pt electrodes on to a quazi-1D nanostructure through the shadow mask. The similarity of the Pd and Pt catalytic properties[29,35] along with statistical variations in the electrochemical properties of Pt/SnO_2 interfaces at near contact areas can provide sufficient diversity in sensitization to enhance the recognition power of such E-nose prototypes.

The performance of one of these wedge-like NB multisensors under real working conditions is illustrated in Figure 3. After standard thermal training very good sensitivity, response time, and stability of the sensing elements were obtained. As an example, upon admission of 1 ppm of isopropyl alcohol vapor in humid air the segments demonstrated 5−10% resistance change. Though the relatively large time constant (~3 min) of the gas delivery system overwhelms the response time of the sensor itself in this particular case (Figure 3a), as fast as 10 s response time (90% of the signal) has been obtained in a better tuned gas delivery setup (see Figure S15 in Supporting Information). As shown in Figure 3b, there are significant variations in sensitivity and optimum operation temperature of the randomly selected NB segments. These variations are too large to be explained by the difference in the morphology of the segments of the same nanobelt and most likely occur due to different catalytic efficiency of the Pt-enriched areas adjacent to the electrodes. Similar to the aforementioned Pd functionalization, near the electrode Pt is a well known catalyst which promotes adsorption and dissociation of oxygen and/or analyte gases and thus significantly reduces the operation temperature of the sensor compared to one made of pristine SnO_2.[29,34,35,39]

The significant diversity in the response to different reducing gases of a single NB multisensor, modified using this simple approach, is demonstrated by the radar plot in Figure 3c. To quantitatively evaluate the analyte-dependent differences of the response of the single NB E-nose we have employed a pattern recognition technique based on the linear discriminant analysis (LDA).[8] This method allows one to transfer the multidimensional sensor signals (in our case, normalized resistances) related to different analytes into an artificial multidimensional feature space where the linear combination of features provides the best separation of the tested analytes. Prior to LDA the input data (resistances)

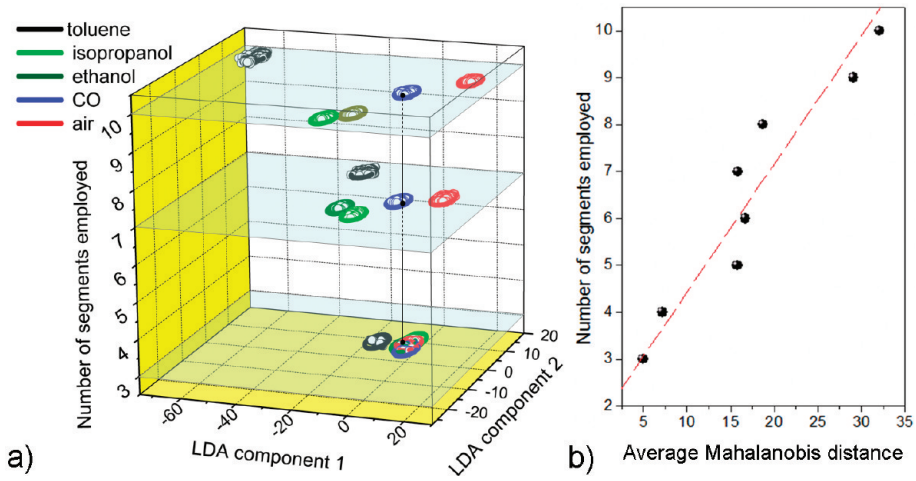

Figure 4. The LDA processing of the response of the single SnO_2 NB E-nose to the binary mixture of humidified (RH = 50%) synthetic air with the analyte at 30 ppm concentration for four gases: ethanol, isopropyl alcohol, toluene, and CO. The NB E-nose operates under homogeneous temperature distribution at T = 290 °C. The classification LDA ellipses correspond to normal distribution of data at 0.99 confidence level. (a) Top LDA plane corresponds to the processing of the response of all the 10 NB segments to 5 gases, including the synthetic air; two other LDA planes have been built under a decreasing number of NB sensor (7 and 3) segments involved in the analysis. (b) The increase of Mahalanobis distance at the LDA feature space between data clusters related to various analytes *vs* number of NB sensor segments involved in the analysis.

are normalized to the median value as $r_i = R_i/R_{med}$. Such data preprocessing increases the stability of recognition by diminishing gas concentration dependency and also compensates possible drift effects. Only the steady-state resistance values recorded at prolonged gas exposure have been taken to carry out the LDA (The details of the application of LDA and MD are provided in Methods and the Supporting Information). The top panel in Figure 4a depicts the LDA plot of component 1 *versus* component 2, calculated for a single NB E-nose where all 10 segments are in operation. As one can see, the multisensor data related to different analytes are clearly separated from each other and the average Mahalanobis distance (MD) between analyte-dependent data clusters at the LDA feature space in this case is about 33 units. Moreover, Figure 4a shows that if three, or even more, sensing segments are failing (and therefore become excluded from the LDA processing) the single NB E-nose is still able to "recognize" the differences between the analytes (middle and lowest shadowed planes in Figure 4a). More quantitatively this "robustness" trend is depicted in Figure 4b where the MD value is plotted as a function of the number of sensing segments employed. As expected, the MD value increases with the number of segments involved to the analysis. However, as can be seen, even five segments are sufficient for confident recognition of the test gases. The latter observations have an important practical consequence: if one or more NB segments eventually fail, the array should still be able to discriminate between different analytes using the initial calibration database. Interestingly, the scattering of the points in Figure 4b also indicates inhomogeneous contribution of different NB segments to the overall recognition of the tested analytes. If the electronic or chemical properties of the different segments in the NB E-nose would be correlated, then the MD between analyte clusters at the LDA space will show a weak dependence on the number of segments employed for the analysis. Therefore, the obtained data additionally prove the sufficiency of the experimental approaches used to differentiate the sensitivity of the different NB segments.

E-nose Performance Tests against the Complex Odors. The real-world applications of E-nose instruments usually deal with significantly more complex odors or aromas, for example, ones widespread in the food industry. To test the performance of the single NB E-Nose (Figure 5a,b) against such complex environments, we exposed it to the vapors from the headspace (Figure 5c) of four alcoholic beverages (glühwein, champagne, vermouth, brandy). To eliminate the strong influence of the different ethanol content to the sensor signal, all beverages were diluted in distilled water to contain the same amount (10 rel. %) of ethanol. The details of measurements are provided in Methods and the Supporting Information. For comparison, the response of NBs to distilled water and 10% water/ethanol mixture were tested as well. Figure 5d shows the radar diagrams of the resistance of all 10 segments (numbered 9−19) of the tested single NB multisensor. As one can see, the diagrams are analyte specific and could allow the aroma identification using the LDA processing (Figure 5e). It should be noticed that well distinguished aroma patterns were observed at the high level of ethanol content in the headspace, which is the dominant component of the sensor signal for any alcoholic beverage. The ability to reliably recognize the aromas of the different beverages illustrated in Figure 5 indicates that the sensitivity of the NB segments to low concentration complex aromatic compounds is sufficient even under the strong

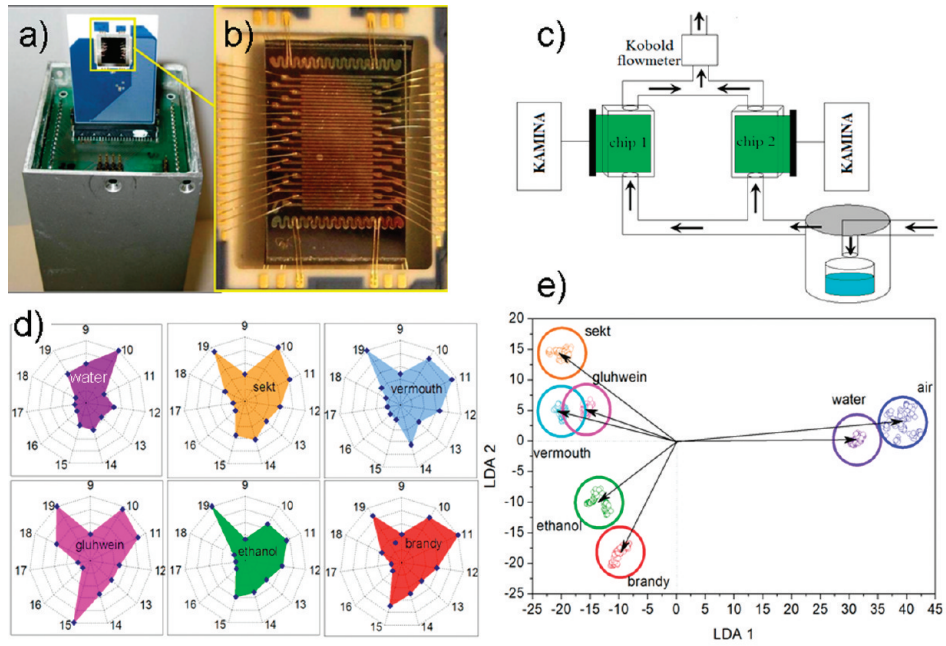

Figure 5. The real-world tests of the single SnO_2 nanobelt E-nose: (a,b) packaged 39-electrode microchip in connection with the KAMINA unit; (c) experimental setup to test the performance of the E-nose; (d) polar plots of the responses of the NB multisensor array to the aroma of various alcohol beverages; (e) corresponding LDA plot of the NB multisensor response to the aromas.

background of ethanol. Different from the case of the simple redox gases, where the wide range of the analyte concentrations can be used in LDA analysis, the sampling of the beverage headspace offers a rather narrow window of concentrations of the vapors in air. The latter is responsible for much smaller scattering in the LDA class ellipsoids. As can be seen in Figure 5b, the NB E-nose responses to less aromatic compounds (*i.e.*, distillated ethanol and brandy) produce the feature clusters which are significantly separated from ones related to spicy wines. At the same time, the influence of water vapor concentration is very moderate, what is characteristic for the conventional metal oxide chemiresistors. As a result, the multisensor data related to water vapor are seen to be close to that of the pure air.

In conclusion, few approaches have been proposed recently to implement metal oxide nanowires as a platform for E-noses.[31−33,41] This article reports on probably the simplest in fabrication and yet excellently performing single SnO_2 NB E-nose system. The approach proposed here demonstrates the potential of combination of bottom-up nanowire fabrication protocols with the state-of-the art microfabrication methods to design prospective simple sensing arrays which, in principle, might be scaled down to the size of few micrometers and thus become the smallest analytical instrument. In addition, the employment of individual single-crystal quasi-1D nanostructure as an active element in a multisensor device is favorable since it allows the fabrication of sensitive, and what is most important for E-nose applications, inherently stable and predictable (calculable) ultrasmall conductometric analytical instruments. The recently reported self-heated metal oxide NB sensors[26,27] open up an additional principal opportunity to reduce the operational power consumption of such devices to 10−20 microwatts level that makes feasible the coupling of analytical and energy harvesting nanodevices in one stand-alone unit.

METHODS

Fabrication of SnO_2 NBs and Their Functionalization. SnO_2 nanobelts were grown by vapor−solid technique at temperatures around 1000 °C using SnO powder as a source material. The wedge-like morphology of the NB was due to reduction of the evaporation rate of the SnO precursor. The deposition of the Pd catalyst (3−10 nm) was performed through the shadow mask on to the thickest part of the nanostructure.[30,40] Individual Pd patches are isolated from each other which precludes surface electrical conductance.

Device Fabrication. Two different approaches have been tested to define electrodes for single crystal SnO_2 NB E-nose. (i) A single NB was placed on to the Si/SiO_2 wafer with a predeposited array of Pt microelectrodes. The NB was electrically bonded to the array using electron beam assisted deposition (EBAD) of Pt from a precursor gas. (ii) Alternatively, the microarray of 7−15 Pt strip electrodes were deposited on to the Si/SiO_2 wafer containing a few prealigned ultralong (500−1500 μm) NBs using R.F. sputtering through the shadow mask. The required temperature distribution over the microarray was defined by Pt meander heaters on the back side of the microchip, and the temperature of the NB array was monitored by 2 thermo-resistors located on the front side of the chip.

Data Acquisition System. The commercially available KAMINA unit (Karlsruhe Institute of Technology) was used to read and process the signal generated by the microarray chip. The sampling rate of the individual segment resistor was *ca.* 1 Hz.

Gas Sensing Measurements. The gas sensing performance of the multisensor array based on individual SnO_2 NB was tested using the calibrated mixtures of test gases in humidified (RH = 50%) synthetic air. The gas flow rate was maintained at the level of 1 L/min. Analyte concentrations have been chosen in the range of 1−50 ppm; the exposure time has been varied in the range of 3−30 min. To measure the response to aroma from headspace of alcohol beverages the custom-made experimental setup included an air generator which supplied a pure dry air from atmosphere and glass bell chamber (*ca.* 150 mL), containing sample liquids. The samples were 1 mL droplets disposed at the Petri dish, 30 × 10 mm^2 inside bell chamber.

The LDA Processing. Linear discriminant analysis (LDA) was used to evaluate the recognition power of the single NB E-nose. Prior to LDA, sensor segments resistance data were normalized to their median value: R_i/R_{med}, where R_i is the resistance of *i*th segment; R_{med} the median resistance value over the sensor array. The only stationary resistance values recorded at each gas exposure have been taken for LDA processing. The LDA classification spheres were calculated with the confidence level of 0.99.

Acknowledgment. The authors are grateful to Dr. J. Goschnik for his enthusiastic support of the pilot project at its early stage. We thank engineers C. Watts (SIUC), J. Benz, G. Stengel, U. Geckle, V. Hermann, and Dr. D. Fuchs (KIT) for their help in designing the parts and XRD/XPS tests as well Prof. D. Usanov (SSU) for useful discussions. V.S. thanks INTAS postdoctoral grant and Fulbright Scholarship for financial support of his stay at SIUC. The SIUC part of the research was supported through a Caterpillar Inc., research grant and at later stages through a NSF ECCS-0925837 grant. S.K. acknowledges support by the Interconnect Focus Center NY at RPI, one of the five FCRPs of SRC.

Supporting Information Available: Details on growth and characterization of SnO_2 NBs, deposition of metal clusters onto the NBs, submicrometer-contact fabrication by electron beam assisted Pt deposition, microelectrode deposition by magnetron sputtering, gas response measurements, experimental setups, and LDA procedure. This material is available free of charge *via* the Internet at http://pubs.acs.org.

REFERENCES AND NOTES

1. Miller, R. A.; Nazarov, E. G.; Eiceman, G. A.; King, A. T. A MEMS Radio-Frequency Ion Mobility Spectrometer for Chemical Vapor Detection. *Sens. Actuators A* **2001**, *91*, 301–312.
2. Mulligan, C. C.; Justes, D. R.; Noll, R. J.; Sanders, N. L.; Laughlin, B. C.; Cooks, R. G. Direct Monitoring of Gaseous Toxic Compounds in Air Using a Portable Mass Spectrometer. *Analyst* **2006**, *131*, 556–567.
3. Lu, C.; Steinecker, W. H.; Tian, W.; Oborny, M. C.; Nichols, J. M.; Agah, M.; Potkay, J. A.; Chan, H. K. L.; Driscoll, J.; Sacks, R. D.; *et al.* First-Generation Hybrid MEMS Gas Chromatograph. *Lab Chip* **2005**, *5*, 1123–1131, and references therein.
4. Firestein, S. How the Olfactory System Makes Sense of Scents. *Nature* **2001**, *413*, 211–218.
5. Shepherd, G. M. Smell Images and the Flavour System in the Human Brain. *Nature* **2006**, *444*, 316–321.
6. Hierlemann, A.; Gutierrez-Osuna, R. Higher-Order Chemical Sensing. *Chem. Rev.* **2008**, *108*, 563–613.
7. Persaud, K.; Dodd, G. Analysis of Discrimination Mechanisms in the Mammalian Olfactory System Using a Model Nose. *Nature* **1982**, *299*, 352–355.
8. Pearce, T. C.; Schiffman, S. S.; Nagle, H. T.; Gardner, J. W., Eds. *Handbook of Machine Olfaction: Electronic Nose Technology*; Wiley-VCH: Weinheim, Germany, 2003.
9. Turner, A. P. F.; Magan, N. Electronic Noses and Disease Diagnostics. *Nat. Rev. Microbiol.* **2004**, *2*, 161–167.
10. Rock, F.; Barsan, N.; Weimar, U. Electronic Nose: Current Status and Future Trends. *Chem. Rev.* **2008**, *108*, 705–725.
11. Sato, K.; Pellegrino, M.; Nakagawa, T.; Nakagawa, T.; Vosshall, L. B.; Touhara, K. Insect Olfactory Receptors are Heteromeric Ligand-Gated Ion Channels. *Nature* **2008**, *452*, 1002–1006.
12. Lundstrom, I.; Erlandsson, R.; Frykman, U.; Hedborg, E.; Spetz, A.; Sundgren, H.; Welin, S.; Winquist, F. Olfactory Images From a Chemical Sensor Using a Light-Pulse Technique. *Nature* **1991**, *352*, 47–50.
13. Grate, J. W.; Rose-Pehrsson, S. L.; Venezky, D. L. Smart Sensor System for Trace Organophosphorus and Organosulfur Vapor Detection Employing a Temperature-Controlled Array of Surface Acoustic Wave Sensors. Automated Sample Preconcentration, and Pattern Recognition. *Anal. Chem.* **1993**, *65*, 1868–1881.
14. Fritz, J.; Baller, M. K.; Lang, H. P.; Rothuizen, H.; Vettiger, P.; Meyer, E.; Guntherodt, H.-J.; Gerber, C.; Gimzewski, J. K. Translating Biomolecular Recognition into Nanomechanics. *Science* **2000**, *288*, 316–318.
15. Dickinson, T. A.; White, J.; Kauer, J. S.; Walt, D. R. A Chemical-Detecting System Based on a Cross-Reactive Optical Sensor Array. *Nature* **1996**, *382*, 697–700.
16. Rakow, N. A.; Suslick, K. S. A Colorimetric Sensor Array for Odour Visualization. *Nature* **2000**, *406*, 710–713.
17. Freund, M. S.; Lewis, N. S. A Chemically Diverse Conducting Polymer-Based "Electronic Nose". *Proc. Natl. Acad. Sci. U.S.A.* **1995**, *92*, 2652–2656.
18. Hagleitner, C.; Hierlemann, A.; Lauge, D.; Kimmer, A.; Kerness, N.; Brand, O.; Baltes, H. Smart Single-Chip Gas Sensor Microsystem. *Nature* **2001**, *414*, 293–296.
19. Cui, Y.; Wei, Q. Q.; Park, H. K.; Lieber, C. M. Nanowire Nanosensors for Highly Sensitive and Selective Detection of Biological and Chemical Species. *Science* **2001**, *293*, 1289–1292.
20. Wang, Z. L., Ed. *Nanowires and Nanobelts of Functional Materials*; Nanowires and Nanobelts: Materials, Properties and Devices, Vol. 2; Kluwer Academic: Boston, MA, 2003.
21. Xia, Y. N.; Yang, P. D.; Sun, Y. G.; Wu, Y. Y.; Mayers, B.; Gates, B.; Yin, Y. D.; Kim, F.; Yan, Y. Q. One-Dimensional Nanostructures: Synthesis, Characterization, and Applications. *Adv. Mater.* **2003**, *15*, 353–389.
22. Heo, Y. W.; Norton, D. P.; Tien, L. C.; Kwon, Y.; Kang, B. S.; Ren, F.; Pearton, S. J.; LaRoche, J. R. ZnO Nanowire Growth and Devices. *Mater. Sci. Eng. R* **2004**, *47*, 1–47.
23. Comini, E.; Baratto, C.; Faglia, G.; Ferroni, M.; Vomiero, A.; Sberveglieri, G. Quasi-One Dimensional Metal Oxide Semiconductors: Preparation, Characterization and Application as Chemical Sensors. *Progr. Mater. Sci.* **2009**, *54*, 1–67.
24. Chen, P. C.; Shen, G. Z.; Zhou, C. W. Chemical Sensors and Electronic Noses Based on 1-D Metal Oxide Nanostructures. *IEEE Trans. Nanotechnol.* **2008**, *7*, 668–682.
25. Patolsky, F.; Timko, B. P.; Yu, G. H.; Fang, Y.; Greytak, A. B.; Zheng, G. F.; Lieber, C. M. Detection, Stimulation, and Inhibition of Neuronal Signals with High-Density Nanowire Transistor Arrays. *Science* **2006**, *313*, 1100–1104.
26. Strelcov, E.; Dmitriev, S.; Button, B.; Cothren, J.; Sysoev, V.; Kolmakov, A. Evidence of the Self-Heating Effect on Surface Reactivity and Gas Sensing of Metal Oxide Nanowire Chemiresistors. *Nanotechnology* **2008**, *19*, 355502.
27. Prades, J. D.; Jimenez-Diaz, R.; Hernandez-Ramirez, F.; Barth, S.; Cirera, A.; Romano-Rodriguez, A.; Mathur, S.; Morante, J. R. Ultralow Power Consumption Gas Sensors Based on Self-Heated Individual Nanowires. *Appl. Phys. Lett.* **2008**, *93*, 123110.
28. McAleer, J. F.; Moseley, P. T.; Norris, J. W.; Williams, D. E.; Tofield, B. C. Tin Dioxide Gas Sensors. Part 2:-The Role of Surface Additives. *J. Chem. Soc., Faraday Trans. 1* **1988**, *84*, 441–457.
29. Schweizer-Berberich, M.; Zheng, J. G.; Weimar, U.; Gopel, W.; Barsan, N.; Pentia, E.; Tomescu, A. The Effect of Pt and Pd Surface Doping on the Response of Nanocrystalline Tin Dioxide Gas Sensors to CO. *Sens. Actuators B* **1996**, *31*, 71–75.
30. Kolmakov, A.; Chen, X.; Moskovits, M. Functionalizing Nanowires with Catalytic Nanoparticles for Gas Sensing Applications. *J. Nanosci. Nanotechnol.* **2008**, *8*, 111–121.
31. Sysoev, V. V.; Goschnick, J.; Schneider, T.; Strelcov, E.;

Kolmakov, A. A Gradient Microarray Electronic Nose Based on Percolating SnO_2 Nanowire Sensing Elements. *Nano Lett.* **2007**, *7*, 3182–3188.
32. Chen, P.; Ishikawa, F. N.; Chang, H.; Ryu, K.; Zhou, C. Nano Electronic Nose: A Hybrid Nanowire/Carbon Nanotube Sensor Array with Integrated Micromachined Hotplates for Sensitive Gas Discrimination. *Nanotechnology* **2009**, *20*, 125503.
33. Sysoev, V. V.; Button, B. K.; Wepsiec, K.; Dmitriev, S.; Kolmakov, A. Toward the Nanoscopic "Electronic Nose": Hydrogen *vs* Carbon Monoxide Discrimination with an Array of Individual Metal Oxide Nano- and Mesowire Sensors. *Nano Lett.* **2006**, *6*, 1584–1588.
34. Yamazoe, N. New Approaches for Improving Semiconductor Gas Sensors. *Sens. Actuators B* **1991**, *5*, 7–19.
35. Batzill, M.; Diebold, U. The Surface and Materials Science of Tin Oxide. *Prog. Surf. Sci.* **2005**, *79*, 47–154.
36. Kolmakov, A.; Potluri, S.; Barinov, A.; Mentes, T. O.; Gregoratti, L.; Nino, M. A.; Locatelli, A.; Kiskinova, M. Spectromicroscopy for Addressing the Surface and Electron Transport Properties of Individual 1-D Nanostructures and Their Networks. *ACS Nano* **2008**, *2*, 1993–2000.
37. Lilach, Y.; Zhang, J. P.; Moskovits, M.; Kolmakov, A. Encoding Morphology in Oxide Nanostructures During Their Growth. *Nano Lett.* **2005**, *5*, 2019–2022.
38. Zemlyanov, D.; Aszalos-Kiss, B.; Kleimenov, E.; Teschner, D.; Zafeiratos, D.; Hävecker, M.; Knop-Gericke, A.; Schlogl, R.; Gabasch, H.; Unterberger, W.; Hayer, K.; Klötzer, B. *In Situ* XPS Study of Pd(111) Oxidation. Part 1: 2D Oxide Formation in 10^{-3} mbar O_2. *Surf. Sci.* **2006**, *600*, 983–994.
39. Cabot, A.; Dieguez, A.; Romano-Rodriguez, A.; Morante, J. R.; Barsan, N. Influence of the Catalytic Introduction Procedure on the Nano-SnO_2 Gas Sensor Performances—Where and How Stay the Catalytic Atoms. *Sens. Actuators B* **2001**, *79*, 98–106.
40. Kolmakov, A.; Klenov, D. O.; Lilach, Y.; Stemmer, S.; Moskovits, M. Enhanced Gas Sensing by Individual SnO_2 Nanowires and Nanobelts Functionalized with Pd Catalyst Particles. *Nano Lett.* **2005**, *5*, 667–673.
41. Baik, J. M.; Zielke, M.; Kim, M. H.; Turner, K. L.; Wodtke, A. M.; Moskovits, M. Tin-Oxide-Nanowire-Based Electronic Nose Using Heterogeneous Catalysis as a Functionalization Strategy. *ACS Nano* **2010**, *4* (6), 3117–3122.